Probing nonlinear rheology layer-by-layer in interfacial hydration water

Bongsu Kim, Soyoung Kwon, Manhee Lee, QHwan Kim, Sangmin An, and Wonho Jhe[1]

Department of Physics and Astronomy, Institute of Applied Physics, Seoul National University, Seoul 151-747, Republic of Korea

Edited by David A. Weitz, Harvard University, Cambridge, MA, and approved November 9, 2015 (received for review July 29, 2015)

Viscoelastic fluids exhibit rheological nonlinearity at a high shear rate. Although typical nonlinear effects, shear thinning and shear thickening, have been usually understood by variation of intrinsic quantities such as viscosity, one still requires a better understanding of the microscopic origins, currently under debate, especially on the shear-thickening mechanism. We present accurate measurements of shear stress in the bound hydration water layer using noncontact dynamic force microscopy. We find shear thickening occurs above $\sim 10^6$ s^{-1} shear rate beyond 0.3-nm layer thickness, which is attributed to the nonviscous, elasticity-associated fluidic instability via fluctuation correlation. Such a nonlinear fluidic transition is observed due to the long relaxation time ($\sim 10^{-6}$ s) of water available in the nanoconfined hydration layer, which indicates the onset of elastic turbulence at nanoscale, elucidating the interplay between relaxation and shear motion, which also indicates the onset of elastic turbulence at nanoscale above a universal shear velocity of ~ 1 mm/s. This extensive layer-by-layer control paves the way for fundamental studies of nonlinear nanorheology and nanoscale hydrodynamics, as well as provides novel insights on viscoelastic dynamics of interfacial water.

nonlinear rheology | hydration layer | shear thickening | elastic turbulence | dynamic force spectroscopy

The rheological nonlinearity of fluids (1–3) is a universal, highly nonequilibrium phenomenon observed in diverse systems ranging from soft materials [e.g., polymeric (1, 4), biological (5, 6), and colloidal (2, 7–9) solution] to terrestrial layers [e.g., Earth's mantle (10)], occurring at extremely high shear rates (1, 2, 11). Although shear thinning (decrease of viscosity) originates from the decrease of particle density correlation (2, 12), shear thickening (4, 7, 8, 13–17) (increase of viscosity) has been understood in various perspectives such as hydrodynamic instability (18) at high Reynolds number (Re) or order–disorder transition (13, 14) at low Re and high Weissenberg number (Wi) [a measure of elasticity of viscoelastic flows (1); see *SI Appendix*, section S1, for nonlinear hydrodynamics formalism based on Re and Wi]. In particular, such a viscoelastic flow with low Re and high Wi exhibits behaviors similar to the inertial turbulence of Newtonian flow, so termed the elastic turbulence (4, 17). Despite extensive studies, however, one still lacks understanding of (*i*) the role of elastic instability in the enhanced flow resistance and (*ii*) the unexplored characteristics of nonlinear rheology at nanoscale.

The hydration water layer (HWL), which is a ubiquitous form of nanoscale water consisting of water molecules tightly bound to ions or hydrophilic surfaces, is a highly viscoelastic fluid showing sluggish relaxation time (19–21) up to 10 μs (22). Better understanding of the HWL dynamics, especially its nonlinear rheology, is increasingly on demand to address diverse processes associated with HWL and to develop related technologies (23, 24). Nonetheless, there have been only a few experiments reported in literature and the representative work was made by Li and Riedo (25), which described the nonlinear viscoelasticity of nanoconfined water and showed shear thinning effects using atomic force microscopy, operated at relatively low shear rate ($<10^4$ s^{-1}) with the fixed one-layer thickness (about 0.4 nm) of HWL. Recently, nonlinear rheology of HWL was also experimentally studied (26), where the results were simply discussed in terms of Wi, without any detailed description of the nonlinear fluidic characteristics such as shear thinning and shear thickening (1, 2, 7).

Here, we (*i*) present precise measurements of the nonlinear rheological properties of HWL, obtained at high shear rate up to $\sim 10^7$ s^{-1} and with layer-by-layer thickness control of HWL (0.3 ∼ 2.0 nm), (*ii*) propose a theoretical model of shear thickening that is attributed to the elastic instability-induced nonlinear fluidity by using the upper-convected Maxwell (UCM) model (1) in combination with the Reynolds method of treating fluctuations in hydrodynamics (18), and (*iii*) discuss the dynamic change of E_{dis}, the dissipated energy due to HWL, with respect to shear stress as an indirect evidence of elastic turbulence. We find good agreement of experiment with theory when one incorporates the nonlinear fluidity due to correlated fluctuations between shear stress and strain rate. Interestingly, it turns out that shear thickening can be described by such a dominant rheological nonlinearity even in the presence of a noticeable change of the intrinsic viscosity of water (27).

Results and Discussion

Dynamic Transition from Linear to Nonlinear Fluidity. Fig. 1*A* shows the experimental schematic, where we used the noncontact, dynamic force microscopy that employs the quartz tuning fork (QTF) (*Materials and Methods*). As the flattened silica tip, oscillating at frequency (ω) and variable shear-oscillation amplitude (A_0), approaches the mica substrate in air, the HWL is formed in the nanogap. Fig. 1 *B* and *C* presents the effective elasticity (k) and damping coefficient (b) of HWL versus the gap separation (y_0), respectively, measured during tip retraction. The data in the green-colored region between $y_0 =$ 0.3 and 2.0 nm

Significance

The hydration water layer (HWL) is a ubiquitous form of nanoscale water bound to the hydrophilic surfaces and plays a critical role in diverse phenomena in nature. Especially, investigation of its nonlinear fluidic properties is important for better understanding of its rheological contributions at a microscopic level. Using precise control and sensitive detection of HWL, we observe shear thickening at above a critical shear-strain rate of 10^6 s^{-1}, resulting from the interplay between relaxation and elasticity-induced fluctuation correlation. Interestingly, the results indicate the occurrence of elasticity turbulence above a universal shear velocity of ∼1 mm/s. This work not only furthers our understanding of nonlinear nanorheology but is a stepping-stone toward controlled experiments on the nonlinear fluid dynamics near the interface.

Author contributions: B.K. and W.J. designed research; B.K., S.K., S.A., and W.J. performed research; M.L. and Q.K. contributed new reagents/analytic tools; B.K., S.K., M.L., Q.K., S.A., and W.J. analyzed data; and B.K. and W.J. wrote the paper.

The authors declare no conflict of interest.

This article is a PNAS Direct Submission.

Freely available online through the PNAS open access option.

[1]To whom correspondence should be addressed. Email: whjhe@snu.ac.kr.

This article contains supporting information online at www.pnas.org/lookup/suppl/doi:10.1073/pnas.1515033112/-/DCSupplemental.

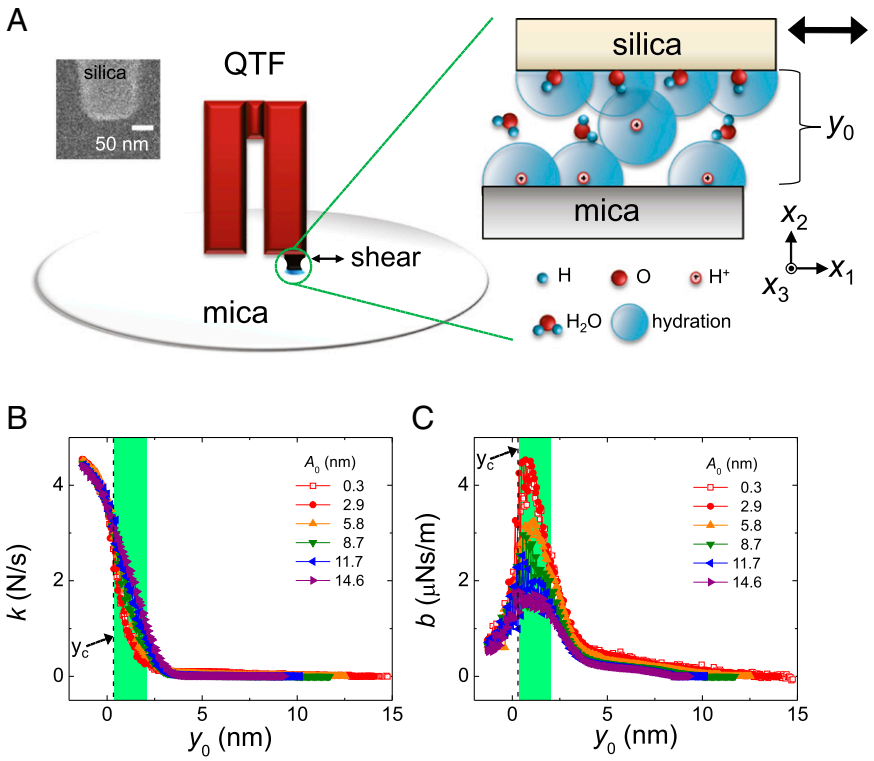

Fig. 1. Dynamic shear viscoelasticity of hydration water layer (HWL). (*A*) Experimental schematic. The HWL is nanoconfined and sheared between the flattened silica tip, attached to the QTF, and the mica surface in ambient condition. The QTF oscillates horizontally in parallel with the mica surface (*Materials and Methods*), which can exert a high shear rate on HWL as well as make a sensitive measurement of the viscoelasticity of HWL. (*B* and *C*) Measured shear elasticity (k) and damping coefficient (b), respectively, versus the tip–mica gap separation (y_0) at various shear oscillation amplitude (A_0). The green-colored region between 0.3 and 2.0 nm indicates the experimental data used for our theoretical analysis of nonlinear rheology, where y_c represents the contact point (*SI Appendix*, section S5). Notice that the data for $A_0 = 0.6$ and 1.5 nm are omitted because they show very similar behaviors to those between $A_0 = 0.3$ and 2.9 nm.

show dramatic variations with A_0 (or equivalently, shear rate), used for our analysis of nonlinear rheology of HWL. Notice that, above $y_0 = 2$ nm, the capillary effects dominate while the HWL effects disappear (28), and the nonlinear rheological properties due to capillarity are detailed in the ref. 27 (as shown in figure 3*A* of ref. 27, the contact line-induced interaction decreases k and b with the increase of A_0). Therefore, whereas the shear thickening of HWL originates from the fluctuation correlation, the capillary effect results in shear thinning, in contrast to HWL, associated with the pinning–depinning dynamics of the capillary contact line (27).

Fig. 2 *A* and *B* presents the data for $y_0 \leq 2$ nm, plotted in terms of the out-of-phase viscosity η'' ($\eta'' \approx ky_0/\Omega$, Ω being the interacting area of the tip) and the dynamic viscosity η' ($\eta' \approx by_0/\Omega$) versus the shear rate $\dot{\gamma}_0$ ($\dot{\gamma}_0 \approx v_{tip}/y_0 \approx A_0\omega/y_0$, v_{tip} being the tip velocity), respectively. Dynamic transition from linear to nonlinear flow is clearly observed: the elastic part (η'') exhibits shear thickening above the critical shear rate of $\sim 10^6$ s^{-1} except for $y_0 = 0.3$ nm (i.e., single molecular layer of water), whereas the viscous part (η') reveals shear thinning even at $y_0 = 0.3$ nm (to be discussed later), which is consistent with the previous results (25).

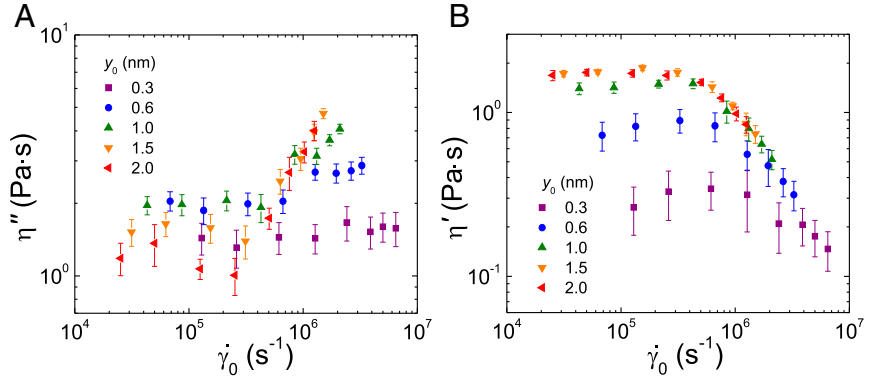

Fig. 2. Dynamic transition from linear to nonlinear flow. (*A* and *B*) Out-of-phase viscosity ($\eta'' \approx ky_0/\Omega$, Ω is the interacting area of the silica tip) and dynamic viscosity ($\eta' \approx by_0/\Omega$) versus the shear rate ($\dot{\gamma} \approx A_0\omega/y_0$), respectively, obtained at various gap distance (y_0). Above the critical shear rate of about 10^6 s^{-1}, there occurs dynamic transition from laminar flow to nonlinear fluidity: the elastic part (η'') shows shear thickening except for $y_0 = 0.3$ nm, whereas the damping part (η') exhibits shear thinning even at $y_0 = 0.3$ nm (see discussion in the text). Each data point represents the average of 12 independent measurements, and its error bar corresponds to 1 SD.

Fig. 3*A* plots the normalized shear stress ratio σ_{21}/σ_0, obtained from Fig. 2, where the total shear stress σ_{21} is proportional to the effective viscosity, $\sqrt{\eta''^2+\eta'^2}$ (σ_0 is the shear stress in the linear flow region). The results evidence enhanced flow resistance above $\dot{\gamma}_0 \sim 10^6\ s^{-1}$ except for $y_0 = 0.3$ nm, demonstrating (*i*) shear thickening (enhancement of flow resistance) at nanoscale and (*ii*) nonlinear rheological characteristics of HWL. Combining the fluctuation-induced fluidic stress and the UCM model of the stress-tensor equation, we now address the physical origin of such nanorheological nonlinearities.

Nonlinear Rheology of Enhanced Flow Resistance in HWL: Theoretical Model. The UCM model (1), an extended formalism of the linear Maxwell model with the upper-convected time derivative, being widely applied for understanding nonlinear rheology of the highly deformed viscoelastic materials, presents the hydrodynamic equation:

$$\boldsymbol{\sigma} + \tau\hat{\boldsymbol{\sigma}} = \eta\left(\nabla\mathbf{v} + (\nabla\mathbf{v})^{\dagger}\right), \qquad [1]$$

$$\hat{\boldsymbol{\sigma}} = \partial_t\boldsymbol{\sigma} + \mathbf{v}\cdot\nabla\boldsymbol{\sigma} - \left\{(\nabla\mathbf{v})^{\dagger}\cdot\boldsymbol{\sigma} + \boldsymbol{\sigma}\cdot(\nabla\mathbf{v})\right\}, \qquad [2]$$

where $\hat{\boldsymbol{\sigma}}$ denotes the convected time derivative of the stress tensor $\boldsymbol{\sigma}$; τ (η), the relaxation time (shear viscosity) in the Maxwell model; and $\nabla\mathbf{v}$, the velocity-gradient tensor with its ij component, $(\partial v_j/\partial x_i)$. Here, the elasticity of the viscoelastic fluid becomes dominant when τ is longer than the reciprocal shear rate (1), $\tau \gg 1/\dot{\gamma}_0$. Notice that Eq. **1** describes the usual hydrodynamic stress tensor if $\tau = 0$, while it becomes the linear Maxwell model when $\hat{\boldsymbol{\sigma}}$ is simply replaced by $\partial_t\boldsymbol{\sigma} = \partial\boldsymbol{\sigma}/\partial t$. Eq. **2** shows that there exists coupling between different components of shear stress $(\boldsymbol{\sigma})_{ij} \equiv \widetilde{\sigma}_{ij}$ and strain rate $(\nabla\mathbf{v} + (\nabla\mathbf{v})^{\dagger})_{ij} \equiv \widetilde{\dot{\gamma}}_{ij}$, which is missing in the linear model.

For the simple shear flow with fluctuations absent, the shear stress in the UCM model takes the asymptotic form in the linear Maxwell model ($t \gg \tau$) (*SI Appendix*, section S2). However, in reality, fluctuations always exist as manifested in the hydrodynamic instability (29) or the shear-induced Brownian motion (30), so that solutions of Eqs. **1** and **2** become very complicated because of mixing between various fluctuating stress and strain rate components. Thus, following the methods developed by Reynolds (18), we decompose the components of stress ($\widetilde{\sigma}_{ij}$) and velocity ($\widetilde{v}_i$) into their mean values (σ_{ij}, v_i) and fluctuations (σ'_{ij}, v'_i); $\widetilde{\sigma}_{ij} = \sigma_{ij} + \sigma'_{ij}$ and $\widetilde{v}_i = v_i + v'_i$. Putting Eq. **2** into [**1**], one obtains the equation of the shear stress σ_{21}:

$$\sigma_{21} + \tau\frac{\partial\sigma_{21}}{\partial t} - \tau\dot{\gamma}_{21}\sigma_{22} - \tau\sum_{k=1}^{3}\left(\langle\sigma'_{2k}\dot{\epsilon}_{k1}\rangle + \langle\dot{\epsilon}_{2k}\sigma'_{k1}\rangle\right) = \eta\dot{\gamma}_{21}, \qquad [3]$$

where $\dot{\epsilon}_{ij} \equiv \partial v'_j/\partial x_i$ denotes the fluctuation of the strain rate associated with v'_j; $\dot{\gamma}_{21} = \partial v_1/\partial x_2$, the average shear rate [for oscillatory shear, $\dot{\gamma}_{21} = \dot{\gamma}_0 \sin\omega t = (A_0\omega/y_0)\sin\omega t$]; and $\langle\ \rangle$, the ensemble average. Notice that, in Eq. **3**,

$$\sigma_{FS} \equiv \tau\sum_{k=1}^{3}\left(\langle\sigma'_{2k}\dot{\epsilon}_{k1}\rangle + \langle\dot{\epsilon}_{2k}\sigma'_{k1}\rangle\right) \qquad [4]$$

represents the additional contribution of the nonlinear fluctuation-induced stress, produced by correlations between fluctuations of strain rate and stress.

Because the fluctuation of stress (σ'_{ij}) can result from coupling between other fluctuating components such as $\dot{\epsilon}_{kl}$ and σ'_{mn} in the UCM model, Eq. **4** can be rewritten in terms of correlations between the strain rate fluctuations (*SI Appendix*, section S3):

$$\begin{aligned}\sigma_{FS} \approx\ & \tau\sum_{k=1}^{3}\left\langle\dot{\epsilon}_{2k}\left[\eta\dot{\epsilon}_{k1} + \tau\sum_{l=1}^{3}\left(2\eta\dot{\epsilon}_{kl}\dot{\epsilon}_{l1} + \cdots\right)\right]\right\rangle \\ & + \tau\sum_{k=1}^{3}\left\langle\left[\eta\dot{\epsilon}_{2k} + \tau\sum_{l=1}^{3}\left(2\eta\dot{\epsilon}_{2l}\dot{\epsilon}_{lk} + \cdots\right)\right]\dot{\epsilon}_{k1}\right\rangle.\end{aligned} \qquad [5]$$

Although, for further development of the still complex expression [**5**], one needs explicit information about $\dot{\epsilon}_{ij}$, we instead simplify by using the linear assumption $|\dot{\epsilon}_{ij}| \approx c_0\dot{\gamma}_0 + O(\dot{\gamma}_0^2)$, which holds for small and isotropic strain rate fluctuations, or equivalently for small coefficient c_0, $c_0 < 1$ (as justified in Fig. 3*B*). Notice that this assumption of isotropic fluctuation breaks down at $y_0 = 0.3$ nm (discussions follow). Consequently, we can derive the total shear stress ratio:

$$\sigma_{21}/\sigma_0 \approx 1 + \left(6\tau c_0^2\dot{\gamma}_0 + 6^2\tau^2 c_0^3\dot{\gamma}_0^2 + 6^3\tau^3 c_0^4\dot{\gamma}_0^3\right), \qquad [6]$$

where $\sigma_0 = \eta\dot{\gamma}_0$ is the linear shear stress. Here, when $\tau \ll 1/\dot{\gamma}_0$, the first term in Eq. **6** is dominant, corresponding to the simple linear flow. Notice that Eq. **6**, which is based on the linear shear motion, can be equally applied to the present oscillatory shear

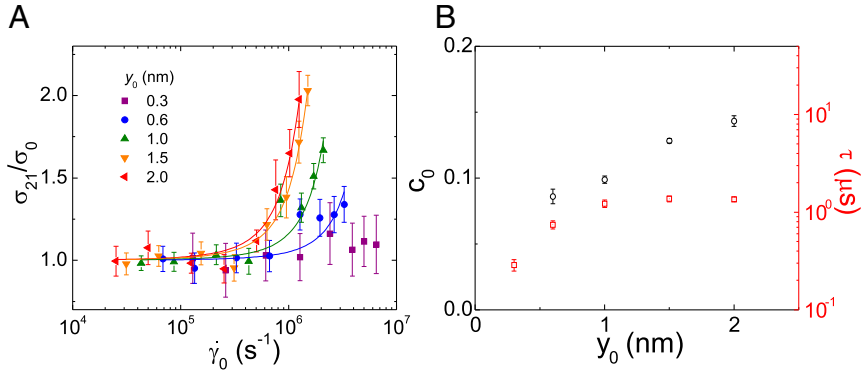

Fig. 3. Nonlinear rheology of enhanced flow resistance in HWL. (*A*) Normalized ratio of shear stress. The stress (σ_{21}) is experimentally obtained by the complex viscosity multiplied by the shear rate. Each colored dataset is well fitted by Eq. **6** except for $y_0 = 0.3$ nm, which corresponds to single layer of water molecules. (*B*) Experimental derivation of c_0 (the measure of fluctuation compared with the mean shear rate) and τ (the position-dependent relaxation time of HWL), obtained by fitting Fig. 2*B*. Notice that, although we made curve fittings while assuming constant shear viscosity of water (η) in Fig. 3*B*, we found only slight increase of c_0 even when the shear-thinning effect (decrease of η in Fig. 2*B*) is included in our formalism (*SI Appendix*, section S3). Extraction of τ from Fig. 2*B* was done in combination with the Carreau–Yasuda model that describes shear thinning (*SI Appendix*, section S4).

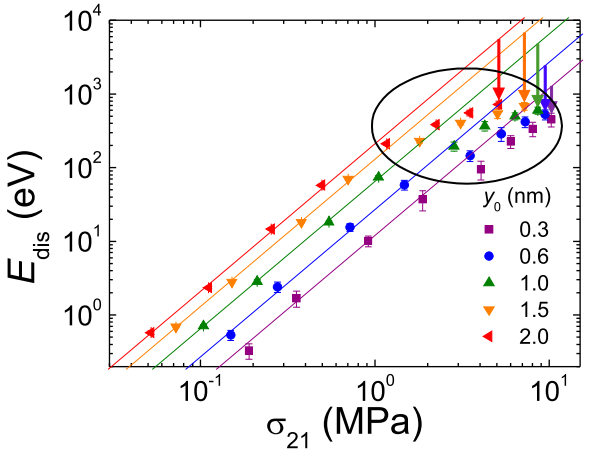

Fig. 4. Energy dissipation and elastic turbulence in HWL. At low shear rate, the dissipated energy E_{dis} by HWL follows the plotted lines, which increase as $\dot{\gamma}_0^2$, and thus the turbulence behavior of HWL does not appear, as described in the ref. 28. At high shear rate, however, the E_{dis} values (circled in ellipse) deviate and decrease with respect to the lines, which shows that a portion of the acquired energy by shear stress is transferred to the turbulent kinetic energy, indicating the occurrence of elastic turbulence in HWL. Notice that the hydrodynamic fluctuations produced by the turbulent kinetic energy results in the additional fluctuation-induced flow resistance as represented by σ_{FS} in Eq. **4**.

experiment because of the relatively low frequency ω (*SI Appendix*, section S2).

Eq. **6** is well fitted to the experimental data given in Fig. 3*A* for each y_0. Here the y_0-dependent τ values are determined from Fig. 2*B* and *SI Appendix*, Fig. S3*A* (*SI Appendix*, section S4). Simulations on HWL between adjacent hydrophilic surfaces, which are interrelated by the hydrogen-bond network, show that (24) the correlation time between hydrogen bonds becomes longer than in bulk water, as observed (19–21) or expected (22) by the sluggish dynamics with a longer τ (Fig. 2*B*). Therefore, shear thickening, resulting from the fluctuation-induced correlation, may be also associated with the similarly "stretched" network that consists of water molecules and HWLs. In Fig. 3*B*, c_0 represents the degree of fluctuation with respect to the mean shear rate and is consistently small (< 1), justifying the assumption used in derivation of Eq. **6**. Importantly, even when one incorporates the shear-thinning effect (decreased η) (Fig. 2*B* and *SI Appendix*, Fig. S3*A*) into Eq. **3**, one still observes very similar behaviors to those with constant η, but with slightly increased c_0 (*SI Appendix*, section S3). Notice that, in the present formalism, shear thinning can be understood as associated with the fluctuation-assisted rapid decrease of particle density correlation (2, 12) under high shear rate, indicating the enhanced molecular escape from the neighboring "cage molecules," which produces the overall molecular mixing in the liquid.

Energy Dissipation and Turbulence in HWL at High Shear Rate. Investigation of dynamical behaviors of the dissipated energy (E_{dis}) can provide an indirect evidence for occurrence of elastic turbulence in HWL at high shear rate, which also supports that the HWL incorporates indeed the hydrodynamic fluctuations as modeled in our analysis. In ref. 28, it is shown in detail that the HWL obtains energy from shear deformation under the shear stress (σ_{21}), which is then dissipated in proportion to $\dot{\gamma}_0^2$ (or v_{tip}^2) at low shear rate and under 2.0-nm thickness. However, if elastic turbulence occurs in the HWL, a portion of the acquired energy by shear stress should be constantly transferred to the turbulent kinetic energy, which is the important characteristics that accompanies turbulence (31), and thus the net dissipated energy of the HWL becomes reduced. This turbulence-induced energy dissipation is shown. In Fig. 4; although the measured E_{dis} increases along the plotted lines, proportional to $\dot{\gamma}_0^2$, at low shear rate, the E_{dis} values at high shear rate (encircled by the ellipse) start deviating and fall below the lines as indicated by each arrow. Notice that the elastic turbulence in the HWL is associated with the turbulent kinetic energy provided by σ_{21}, whose magnitude is the difference between the plotted line and the measured E_{dis}, and the resulting hydrodynamic fluctuations in the turbulent flow induce the additional fluctuation-induced shear stress σ_{FS} (Eq. **4**).

Discussion

Now let us discuss the limiting case of $y_0 = 0.3$ nm (Fig. 2), where the apparent viscosity does not exhibit any shear thickening while the viscous part still shows shear thinning. This remarkable observation demonstrates indeed that our model works consistently with the experiment: at $y_0 = 0.3$ nm where the tightly confined water monolayer is sheared, the strain rate fluctuation vanishes in the vertical y direction ($i,j = 2$) while its horizontal components remain. Consequently, whereas the additional shear stress (Eq. **5**) responsible for shear thickening vanishes, the shear-thinning effect associated with shear viscosity still persists, as previously investigated theoretically (2, 12). Moreover, fluctuations in the vertical direction should increase with y_0 beyond 0.3 nm, as indicated by the gradual increase of c_0 (Fig. 3*B*).

Fig. 5 shows that shear thickening of HWL follows the universal velocity dependence when plotted versus shear velocity (except for $y_0 = 0.3$ nm) instead of shear rate. This remarkable behavior implies that the unique critical velocity of about 1 mm/s may play a fundamental role in the nanorheological phenomena of HWL; for example, the autoregulated velocity ($\sim$1 mm/s) of the deformable red blood cells in the capillary flow of animals may be hinted by the effectively similar nonlinear nanorheology effect of plasma in the narrow gap between blood cell and capillary wall (32).

Last, we emphasize that our theoretical model can be similarly applied to various other viscoelastic liquids under hydrodynamic instability because the model is based on the hydrodynamics with nonlinear stress–strain tensor, namely the UCM model. For example, the colloidal particle system is well suited to our model because it also involves the hydrodynamic instability (at high Wi

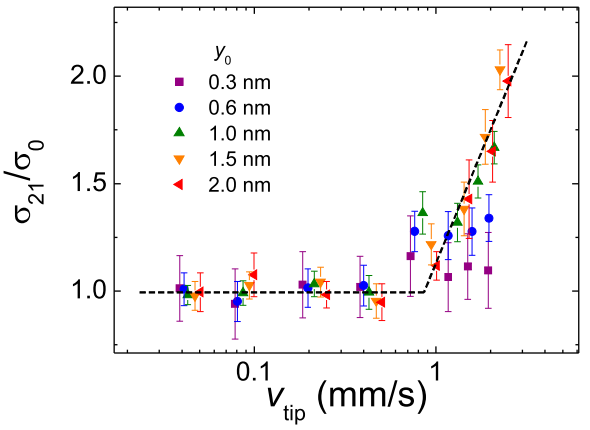

Fig. 5. Universal tip velocity dependence of shear stress enhancement. The normalized shear stress ratio exhibits the universal behavior of stress enhancement, when plotted in terms of the tip velocity, above the critical velocity of about 1 mm/s, except for $y_0 = 0.3$ nm. This indicates that the unique critical velocity ($\sim$1 mm/s) may play a fundamental and ubiquitous role in the nanorheological phenomena associated with the nanometrically thin HWL.

or Péclet number) for shear thickening to occur, irrespective of the contribution of order–disorder transition (7, 9). It is, however, inappropriate to use our model for shear thickening originated from shear-induced structuring such as in surfactant solution (33).

In summary, we have proposed shear thickening can originate from the nonlinear hydrodynamic instability due to fluctuation correlations without involving increase of shear viscosity, as demonstrated in the elasticity-induced enhancement of apparent viscosity in HWL. The broad dynamic range of control and measurement demonstrated in this (sub)nanometric system enables the direct quantitative study of fundamental processes in nonlinear nanorheology of the interfacial water, offering grounds for further studies of, e.g., elastic turbulence at nanoscale or interfacial H-bond dynamics.

Materials and Methods

We measured the rheological properties of the nanometric HWL formed in ambient condition between the flattened fused-quartz silica tip and the mica substrate using the QTF (34). The QTF, when operated in the shear mode (28, 35) of dynamic force microscope, allows accurate noncontact measurements at precisely controlled tip-sample separation due to its high stiffness ($\sim 2 \times 10^4$ N/m) and high quality factor ($\sim 10^4$), oscillating at various amplitudes ($0.3 \sim 14.6$ nm). As detailed in ref. 28, the tip was strongly epoxied to QTF and made flattened (diameter of the flat area is 60 ± 5 nm) while the cleaned mica was tightly fixed on the piezoelectric transducer using an adhesive glue. The silica tip and mica are atomically flat with the root-mean-squared roughness (28) of 0.014 and 0.039 nm (or the corresponding peak-to-peak roughness of about 0.07 and 0.11 nm) on a scanned area of 100×100 nm, respectively. All of the experiments were performed at room temperature (297.5 ± 1 K) and at a high relative humidity of $76.4 \pm 2\%$ where the capillary effects are negligible below 2 nm (28) (notice that the capillary effects, dominant beyond 2 nm separation, are fully described for the water nanomeniscus in ref. 27). Determination of the contact point is given in *SI Appendix*, section S5. For the critical parallelism alignment between tip and substrate, we used a fine tilt stage: in the presence of tilt, the capillary effects become noticeable producing the negative phase signal, which is adjusted to minimize the tilt (*SI Appendix*, section S6).

ACKNOWLEDGMENTS. This work was supported in part by National Research Foundation of Korea Grant 2011-0029541 funded by the Government of the Republic of Korea (MSIP).

1. Bird RB, Armstrong RC, Hassager O (1987) *Dynamics of Polymeric Liquids: Volume 1, Fluid Mechanics* (Wiley-Interscience, New York).
2. Larson RG (1999) *The Structure and Rheology of Complex Fluids* (Oxford Univ Press, New York).
3. Bureau L (2010) Nonlinear rheology of a nanoconfined simple fluid. *Phys Rev Lett* 104(21):218302.
4. Groisman A, Steinberg V (2000) Elastic turbulence in a polymer solution flow. *Nature* 405(6782):53–55.
5. Kollmannsberger P, Fabry B (2011) Linear and nonlinear rheology of living cells. *Annu Rev Mater Res* 41:75–97.
6. Qiu T, et al. (2014) Swimming by reciprocal motion at low Reynolds number. *Nat Commun* 5:5119.
7. Brader JM (2010) Nonlinear rheology of colloidal dispersions. *J Phys Condens Matter* 22(36):363101.
8. Brown E, Jaeger HM (2014) Shear thickening in concentrated suspensions: Phenomenology, mechanisms and relations to jamming. *Rep Prog Phys* 77(4):046602.
9. Wagner NJ, Brady NF (2009) Shear thickening in colloidal dispersions. *Phys Today* 62(10):27–32.
10. Asaadi N, Ribe NM, Sobouti F (2011) Inferring nonlinear mantle rheology from the shape of the Hawaiian swell. *Nature* 473(7348):501–504.
11. Evan DJ, Morriss G (2008) *Statistical Mechanics of Nonequilibrium Liquids* (Cambridge Univ Press, Cambridge, UK), 2nd Ed.
12. Henrich O, Weysser F, Cates ME, Fuchs M (2009) Hard discs under steady shear: Comparison of Brownian dynamics simulations and mode coupling theory. *Philos Trans A Math Phys Eng Sci* 367(1909):5033–5050.
13. Hoffman RL (1972) Discontinuous and dilatant viscosity behavior in concentrated suspensions I. Observation of a flow instability. *Trans Soc Rheol* 16(1):155–173.
14. Laun HM, et al. (1992) Rheological and small angle neutron scattering investigation of shear-induced particle structure of concentrated polymer dispersions submitted to plane Poiseuille and Couette flow. *J Rheol (NY NY)* 36(4):743–787.
15. Groisman A, Steinberg V (2001) Efficient mixing at low Reynolds numbers using polymer additives. *Nature* 410(6831):905–908.
16. Pan L, Morozov A, Wagner C, Arratia PE (2013) Nonlinear elastic instability in channel flows at low Reynolds numbers. *Phys Rev Lett* 110(17):174502.
17. Zhang HN, Li FC, Cao Y, Kunugi T, Yo B (2013) Direct numerical simulation of elastic turbulence and its mixing-enhancement effect in a straight channel flow. *Chin Phys B* 22(2):024703.
18. Reynolds O (1895) On the dynamical theory of incompressible viscous fluids and the determination of the criterion. *Philos Trans R Soc Lond A* 186:123–164.
19. Kim B, et al. (2013) Unified stress tensor of the hydration water layer. *Phys Rev Lett* 111(24):246102.
20. Kim B, Kwon S, Moon G, Jhe W (2015) Shear-stress function approach of hydration layer based on the Green-Kubo formula. *Phys Rev E Stat Nonlin Soft Matter Phys* 91(3):032307.
21. Zhu Y, Granick S (2001) Viscosity of interfacial water. *Phys Rev Lett* 87(9):096104.
22. Leng Y, Cummings PT (2006) Shear dynamics of hydration layers. *J Chem Phys* 125(10):104701.
23. Israelachvili J, Wennerström H (1996) Role of hydration and water structure in biological and colloidal interactions. *Nature* 379(6562):219–225.
24. Leng Y, Cummings PT (2005) Fluidity of hydration layers nanoconfined between mica surfaces. *Phys Rev Lett* 94(2):026101.
25. Li TD, Riedo E (2008) Nonlinear viscoelastic dynamics of nanoconfined wetting liquids. *Phys Rev Lett* 100(10):106102.
26. Kapoor K, Amandeep, Patil S (2014) Viscoelasticity and shear thinning of nanoconfined water. *Phys Rev E Stat Nonlin Soft Matter Phys* 89(1):013004.
27. Lee M, Kim B, Kim J, Jhe W (2015) Noncontact friction via capillary shear interaction at nanoscale. *Nat Commun* 6:7359.
28. Kim B, Kwon S, Mun H, An S, Jhe W (2014) Energy dissipation of nanoconfined hydration layer: Long-range hydration on the hydrophilic solid surface. *Sci Rep* 4:6499.
29. Khujadze G, Oberlack M, Chagelishvili G (2006) Direct numerical simulation of stochastically forced laminar plane Couette flow: Peculiarities of hydrodynamic fluctuations. *Phys Rev Lett* 97(3):034501.
30. Ziehl A, Bammert J, Holzer L, Wagner C, Zimmermann W (2009) Direct measurement of shear-induced cross-correlations of Brownian motion. *Phys Rev Lett* 103(23):230602.
31. Tennekes H, Lumley JL (1972) *A First Course in Turbulence* (The MIT Press, Cambridge, MA).
32. MacVicar BA, Salter MW (2006) Neuroscience: Controlled capillaries. *Nature* 443(7112):642–643.
33. Arai N, Yasuoka K, Zeng XC (2012) Nanochannel with uniform and Janus surfaces: Shear thinning and thickening in surfactant solution. *Langmuir* 28(5):2866–2872.
34. Giessibl F (2003) Advances in atomic force microscopy. *Rev Mod Phys* 75:949–983.
35. Lee M, Sung B, Hashemi N, Jhe W (2009) Study of a nanoscale water cluster by atomic force microscopy. *Faraday Discuss* 141:415–421, discussion 443–465.